



Cite this: *Metallomics*, 2015,
7, 622

Response of CnrX from *Cupriavidus metallidurans* CH34 to nickel binding

Antoine P. Maillard,^{†a} Sandra Künnemann,^{†b} Cornelia Große,^b Anne Volbeda,^a Grit Schleuder,^b Isabelle Petit-Härtlein,^a Eve de Rosny,^a Dietrich H. Nies^b and Jacques Covès^{‡*a}

Resistance to high concentration of nickel ions is mediated in *Cupriavidus metallidurans* by the CnrCBA transenvelope efflux complex. Expression of the *cnrCBA* genes is regulated by the transmembrane signal transduction complex CnrYXH. Together, the metal sensor CnrX and the transmembrane antisigma factor CnrY control the availability of the extracytoplasmic function sigma factor CnrH. Release of CnrH from sequestration by CnrY at the cytoplasmic side of the membrane depends essentially on the binding of the agonist metal ion Ni(II) to the periplasmic metal sensor domain of CnrX. CnrH availability leads to transcription initiation at the promoters *cnrYp* and *cnrCp* and to the expression of the genes in the *cnrYXHCBA* nickel resistance determinant. The first steps of signal propagation by CnrX rely on subtle metal-dependent allosteric modifications. To study the nickel-mediated triggering process by CnrX, we have altered selected residues, F66, M123, and Y135, and explored the physiological consequences of these changes with respect to metal resistance, expression of a *cnrCBA-lacZ* reporter fusion and protein production. M123C- and Y135F-CnrXs have been further characterized *in vitro* by metal affinity measurements and crystallographic structure analysis. Atomic-resolution structures of metal-bound M123C- and Y135F-CnrXs showed that Ni(II) binds two of the three canonical conformations identified and that Ni(II) sensing likely proceeds by conformation selection.

Received 11th November 2014,
Accepted 19th January 2015

DOI: 10.1039/c4mt00293h

www.rsc.org/metallomics

Introduction

Nickel ions are needed as essential cofactors only in a limited number of proteins^{1,2} such as urease, hydrogenases, glyoxalase and some superoxide dismutases. Nickel ions are also toxic even at environmentally relevant concentrations. Proposed mechanisms of nickel toxicity were recently reviewed³ and the zinc-containing enzyme fructose-1,6-bisphosphate aldolase was identified as a specific target.⁴ In contrast, Co(II) ions have no clear physiological role except as a component of vitamin-B12 or as a cofactor in a few noncorrin-cobalt-containing enzymes.⁵ On the other hand, the toxic action of Co(II) has been related to interference with iron-sulfur-cluster biosynthesis.^{6–9} Because the cations of cobalt and nickel may interfere with the anabolic functions of the two most important essential transition metal cations, zinc and iron, bacterial cells might have down-scaled

the use of nickel and treat cobalt essentially as a toxic compound. In *E. coli*, these roles are assumed by transcriptional regulators such as NikR or RncR, that are specific *in vivo* for their cognate metal ions.^{10–15}

In *Cupriavidus metallidurans* CH34, an aerobic β -proteobacterium that prevails in heavy-metal rich environments, surplus cytoplasmic nickel, which has entered the cell through a battery of redundant uptake systems with low substrate specificity,¹⁶ is removed from the cytoplasm by the exporters CnrT and DmeF,¹⁷ and from the periplasm by the RND-driven transenvelope system CnrCBA.¹⁸ The CnrCBA transenvelope complex is predominantly involved in nickel resistance^{19–21} and serves as a back-up system of CzcCBA with respect to cobalt resistance.²² The setup of both the heavy-metal efflux pump CnrCBA and the cation diffusion facilitator CnrT is regulated by the three-protein complex CnrYXH.^{18,20,23,24} The corresponding genes are organized as the *cnrYXHCBA* determinant borne by the megaplasmid pMOL28. Expression of the *cnr* determinant depends on the availability of the extracytoplasmic function (ECF) sigma factor CnrH to substitute for the primary sigma factor on the RNA polymerase.¹⁸ This gives the RNA polymerase the specificity for transcription initiation at the *cnr* promoters, *cnrYp* and *cnrCp*.^{20,24} At the resting state, CnrH is sequestered at the membrane by the anti-sigma protein CnrY.²⁵ Binding of nickel to CnrXs, the periplasmic sensor domain of CnrX, frees CnrH

^a Institut de Biologie Structurale, UMR 5075 CNRS-CEA-Université Grenoble-Alpes, 71, Avenue des Martyrs, 38044 Grenoble Cedex 9, France

^b Institute for Biology/Microbiology, Kurt-Mothes-Str. 3, Martin-Luther-University, 06099 Halle/Saale, Germany

[†] Both authors contributed equally to this work.

[‡] Institut de Biologie Structurale, Campus EPN, CS 10090, 71, Avenue des Martyrs, 38044 Grenoble Cedex 9, France. Email: jacques.coves@ibs.fr; Fax: +33-4-76-50-18-90; Tel: +33-4-57-42-85-16

from CnrY sequestration by a still unknown mechanism.^{21,24–26} Nickel sensing by CnrX is thus a key event in nickel homeostasis in *C. metallidurans*. Expression of *cnrCBA* is mainly induced by nickel ions with a half maximum expression at 50 μM Ni(II) and maximum expression at 0.3 mM Ni(II). Cobalt ions induce to a much lower maximum expression level and three- to six-fold less efficient than nickel ions.^{20,24} Copper is a very poor inducer and zinc ions have no effect at all.^{19,20,24} Actually, in the resting state of the CnrYXH complex, zinc ions likely bind CnrX in a 3N₂O (3 histidines, 1 glutamate) coordination sphere. Due to a better affinity for CnrX, nickel or cobalt can displace the zinc ions at the metal binding site.^{21,26} Their agonist effect was explained by their ability to recruit the only methionine of CnrXs (M123) as an additional ligand, with the shorter the thioether sulfur–metal distance, the better the biological response (Ni > Co > Cu).²¹ Moving from a trigonal bipyramidal geometry in the Zn-bound form to an octahedral coordination sphere in the Ni- or Co-bound form triggers allosteric modifications of the sensor domain, further illustrating the concept of discrimination of cognate from non-cognate metals by ligand selection (number/geometry) linked to allosteric switching.^{27–29} The role of M123 as a trigger of the signal transduction was also highlighted by *in vivo* studies and affinity measurements pointed out the crucial role of this residue in the selectivity of cobalt, compared to zinc.²⁶

The present report improves our understanding of nickel perception and signal propagation by the sensor protein in the CnrYXH complex. By a combination of structural (X-ray crystallography), biochemical, and physiological studies, we have further characterized the contribution of the nickel ligand M123 and we have explored the contribution of the neighboring non-coordinating Y135 or F66 to the nickel-mediated switching process. The specificity of nickel *versus* cobalt is also discussed.

Experimental

Design of the *in vivo* experiments

Genetic techniques, bacterial strains, growth conditions and induction experiments were extensively described previously.^{18,20,23,24,26} Briefly, to characterize *in vivo* their influence on both nickel binding and signal propagation, mutations were introduced at the codons of F66, M123 or Y135 of the *cnrX* gene. The mutated *cnrYXH* operon was cloned into plasmid pBBR1-MCS2 and transferred into *C. metallidurans* strain DN190 (pMOL28-3, $\Phi(\text{cnrCBA-lacZ})\Delta\text{cnrYXH}$). The bacterial strain DN190 is a derivative of *C. metallidurans* AE126 that contains a derivative of pMOL28 and is devoid of pMOL30 to avoid *czc* interference with *cnr* when assessing cobalt resistance. Two types of situations were explored. In the situation named “Yp – Zp”, *cnrYXH* and *cnrCBA-lacZ* were under the control of CnrH-dependent promoters, to be expressed only when CnrH is made available in the cytoplasm. In the “Yp + Zp” situation, the *cnrYXH* operon is under control of *lacZp*, which is constitutive in *C. metallidurans* and should mediate constitutive expression of *cnrYXH* in addition to any transcription initiation starting in a CnrH-dependent manner from *cnrYp*. The “Yp + Zp” situation thus allows uncoupling the

production of the CnrYXH complex from the presence of an inducing metal ion and the CnrH-dependent production of both the efflux pump mediating metal resistance and the β -galactosidase. This orientation can thus be used to verify stability of the CnrX mutant proteins and if expression of *cnrCBA* might be due to a compromised binding of CnrH to the CnrY anti-sigma protein. This experimental setting has already been described and proved to be effective.²⁶ Tris-buffered mineral salts medium containing 2 g sodium gluconate L⁻¹ (TMM) was used to cultivate these strains aerobically with shaking at 30 °C.³⁰ Analytical grade salts of heavy metal chlorides were used to prepare 1 M stock solutions, which were sterilized by filtration. Solid Tris-buffered media contained 20 g agar L⁻¹. For the minimum inhibitory concentration (MIC) determination, the cells were cultivated in TMM for 30 h at 30 °C with shaking, diluted 20-fold into fresh TMM, cultivated for another 24 h, diluted 100-fold into fresh TMM, streaked onto TMM plates containing increasing concentrations of nickel or cobalt chloride and incubated for 5 days at 30 °C.

For conjugative gene transfer, standard molecular genetic techniques were used.^{31,32} Overnight cultures of donor strain *E. coli* S17/1³³ and of the *C. metallidurans* recipient strains grown at 30 °C in Tris-buffered medium were mixed (1 : 1) and plated onto nutrient broth agar. After 2 days, the bacteria were suspended in TMM, diluted, and plated onto selective media as previously described.³¹

For induction experiments, *C. metallidurans* cells with a *lacZ*-reporter gene fusion were cultivated in TMM with shaking at 30 °C. At a cell density of 60–70 Klett units, heavy metal salts were added to various final concentrations and cells were incubated with shaking for additional 3 h. The specific β -galactosidase activity was determined in permeabilized cells as published previously with 1 U defined as the activity forming 1 nmol of *o*-nitrophenol per min at 30 °C.³⁴

For Western-blot analysis, cells were grown in TMM for 30 h at 30 °C with shaking, diluted 200-fold into fresh TMM, divided into two sub-cultures, and cultivated for another 24 h without added metal or in the presence of 0.5 mM NiCl₂. Cells were harvested by centrifugation (2 min, 16 000 \times g, 4 °C) and suspended in buffer (100 mM Tris-HCl, pH 8.0). Crude extracts from 35 μg dry mass of cells were separated by 15% (w/v) SDS-PAGE, blotted onto a PVDF membrane, and visualized using a polyclonal anti-CnrXs antibody. Blots were analyzed by ImageJ (imagej.nih.gov/ij).

Site-directed mutagenesis and protein preparation

The H32A-CnrXs mutant that contains only the physiologic metal-binding site was characterized as a model of the wild-type protein (WT in the following).^{21,26} Consequently, extra mutations were introduced in the H32A background and the over-expression plasmid pET-H32A-CnrXs was used as a matrix to produce the H32A-Y135F double-mutation in CnrXs. The forward and reverse primer sequences for the M123A and M123C mutations were already described.²⁶ Those for the Y135F mutations were GGAAC ATCGACCTGCTTTCGATCGCGTTCCTATC and GATAAGAACGCG ATCGAAGCAGGTCGATGTTCC, respectively. The mismatch positions corresponding to the replacement of the TAC codon (Tyr) by

TTC (Phe) are underlined. QuikChange™ Site-Directed Mutagenesis kit from Stratagene was used as specified by the manufacturer. Mutations were confirmed by DNA sequencing and the new constructs were transformed into *E. coli* BL21(DE3). H32A-Y135F-CnrXs was overproduced and purified as previously described for the other CnrXs proteins.²¹ Protein concentrations were determined using the Bradford protein assay (BioRad) with bovine serum albumin as standard.³⁵

Affinity measurements

The affinity of the protein used in this study for Ni(II) was determined by competition experiments with chromogenic chelators as previously described.²⁶ Mag-fura-2 was used for H32A-M123C- and H32A-M123A-CnrXs while fura-2 was the competitor in the case of H32A-CnrXs (wild-type like) or H32A-Y135F-CnrXs. Mag-fura-2 and fura-2 isotherms were fit to a single site model using the program Dynafit.³⁶ For mag-fura-2/Ni, we used the dissociation constant of 13×10^{-7} M reported in the literature.³⁷ The dissociation constant of fura-2/Ni was determined experimentally to 3.8×10^{-12} M by a competition assay with EGTA using the single model and a K_d of 5.15×10^{-11} M at pH 7.5 for EGTA/Ni.

Crystallization, structure determination and refinement

Crystals were obtained by mixing 1 μ L of protein solution loaded with 4 Ni(II) or Co(II) equiv., with 1 μ L of solution consisting of 1.1–1.2 NaH₂PO₄/0.4 M KH₂PO₄/0.1 M Hepes pH 7.5 for H32A-Y135F-CnrXs or 30% PEG 3350/0.2 M (NH₄)₂SO₄/0.1 M Hepes pH 7.5 for H32A-M123C-CnrXs. Prior to data collection, crystals were harvested in a loop and flash cooled in liquid nitrogen using Paratone-N as a cryoprotectant. Diffraction data were collected at beamline BM30a (ESRF-Grenoble) and integrated with the XDS package.³⁸ The Y135F and M123C mutant crystallized in a tetragonal (*P*₄,2,2) and an orthorhombic (*C*222₁) space group, respectively (Table 1). Two data sets were collected from the same crystal of the M123C mutant, using a three times shorter exposure time for the second one in order to prevent saturation of strong reflections, before scaling and merging them with the XSCALE program of the XDS package. Scaling and merging of diffraction data of the Co-complex of the Y135F mutant was also done with XSCALE, but for the Ni-complex of this mutant the program SCALA from the CCP4 package was used.³⁹ The latter two data sets were very similar, as indicated by an R_{scale} factor of 16.6%, determined by the CCP4 program SCALEIT. Further data statistics are given in Table 1.

The crystal structures were solved by molecular replacement (MR), using the program PHASER.⁴⁰ For Ni-bound Y135F-CnrXs, the WT structure (pdb code 2Y39) was used as the starting model. For the other two structures, MR was started from the refined Ni-bound Y135F-CnrXs model. Refinement of positions (*xyz*) and anisotropic temperature factors (B_{an}) of individual atoms of the latter was started with PHENIX⁴¹ and finished with REF MAC⁴² using the Friedel pairs *F*(+) and *F*(−) as independent observations, thus taking into account the weak anomalous signal of S and Ni atoms. Merged Friedel pairs were used as observations for *xyz* B_{an} (i) refinement of Co-bound Y135F-CnrXs and the Ni-bound M123C mutant. Because the Co-bound Y135F-CnrXs crystal was a bit

Table 1 X-ray data and refinement statistics

| CnrXs mutant | Y135F | Y135F | M123C |
|--|----------------------------|----------------------------|---------------------------|
| Bound metal | Ni | Co | Ni |
| Crystal space group | <i>P</i> ₄ ,2,2 | <i>P</i> ₄ ,2,2 | <i>C</i> 222 ₁ |
| Cell dimensions: <i>a</i> (Å) | 32.40 | 32.42 | 43.91 |
| <i>b</i> (Å) | 32.40 | 32.42 | 47.52 |
| <i>c</i> (Å) | 195.33 | 196.10 | 193.74 |
| Molecules/asymmetric unit | 1 | 1 | 2 |
| X-ray data | | | |
| Overall resolution (Å) | 32–1.11 | 20–1.11 | 25–1.10 |
| Unique reflections | 42 584 | 42 712 | 81 401 |
| R_{sym} (%) | 8.9 | 10.3 | 8.3 |
| $\langle I/\sigma_1 \rangle$ | 12.7 | 12.2 | 16.0 |
| Data completeness (%) | 100.0 | 99.3 | 98.4 |
| High-resolution shell (Å) | | | |
| CC _{1/2} (%) | 1.17–1.11 | 1.18–1.11 | 1.16–1.10 |
| R_{sym} (%) | 92.4 | 82.8 | 78.2 |
| $\langle I/\sigma_1 \rangle$ | 32.7 | 59.6 | 58.6 |
| Data completeness (%) | 5.3 | 3.1 | 3.5 |
| | 100.0 | 96.0 | 96.6 |
| Refinement | | | |
| Resolution range (Å) | 30–1.11 | 20–1.30 | 24.8–1.10 |
| Reflections used for R_{work} | 40 322 | 25 670 | 77 363 |
| Reflections used for R_{free} | 1980 | 1430 | 4038 |
| Number of non-H atoms | 1266 | 1266 | 2541 |
| Number of H atoms | 1025 | 1021 | 2188 |
| R_{work} (%) | 10.8 | 13.0 | 11.5 |
| R_{free} (%) | 12.4 | 17.2 | 14.5 |
| σ_{bond} (Å) | 0.013 | 0.011 | 0.016 |
| σ_{angle} (°) | 1.7 | 1.5 | 1.8 |
| $\langle B \rangle$ (Å ²) | 8.8 | 12.3 | 13.9 |

overexposed to X-rays and no low-resolution data set was collected here, the resolution was limited at 1.3 Å for refinement in order to obtain satisfactory statistics. The other structures were refined at 1.11 (Ni-bound Y135F-CnrXs) and 1.10 Å (Ni-bound M123C-CnrXs) resolution (see Table 1 for refinement statistics). Manual corrections, where necessary, were performed with COOT.⁴³ Hydrogen atoms were added by REF MAC and included in the refinement without manual intervention. No ligand restraints were used for the metal sites except that the Van der Waals radii of Ni and Co were decreased in order to prevent ligand repulsion in the refinement. Coordinates and structural factors for Ni-bound and Co-bound Y135F-CnrXs, and for Ni-bound M123C-CnrXs have been deposited in the Protein Data Bank with accession number: 4WWB, 4WWD and 4WWF, respectively.

Results

Physiological consequences of the mutations.

The phenotype of the M123C, F66A and Y135F derivatives of CnrX was assessed in *C. metallidurans* CH34 as previously described.²⁶ The results are expressed in Fig. 1 as the specific β -galactosidase activity in the absence of inducing metal (white columns), and then in the presence of 0.5 mM Ni(II) recorded every 30 min until 3 h and reported as the variation averaged for 3 h (grey columns), the presence of CnrX revealed by Western-blot, depending on the presence of Ni(II) or not, and finally the minimum inhibitory concentration (MIC) of Ni(II) and Co(II).

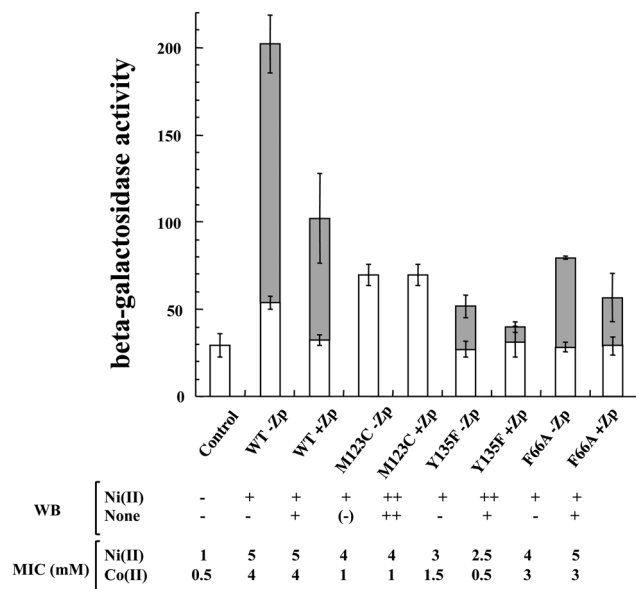


Fig. 1 *In vivo* effects of the mutations. *C. metallidurans* strain DN190(pMOL28-3 Δ *cnrYXH* Φ *cnrCBA-lacZ*), additionally containing a pBBR derivative with no insert (control) or with the mutated *cnrYXH* region in “Yp + Zp” (+Zp) or in “Yp – Zp” (–Zp) orientation was cultivated in TMM for 30 h at 30 °C, diluted to 30 Klett units with fresh TMM, and incubated with shaking until the turbidity reached 60 Klett units. This culture was divided into sub-cultures that were incubated with shaking at 30 °C in the presence of 0.5 mM Ni(II) or no metal. Samples were removed every 0.5 h until 3 h were reached, and the specific β -galactosidase activity in U mg^{–1} dry mass was determined. Each experiment was performed three or four times. Results are expressed as a histogram in which white columns represent the specific β -galactosidase activity recorded right before addition of nickel, and gray columns represent the nickel-dependent increase in specific β -galactosidase activity averaged for 3 h. The absence of gray column means that no significant Ni-dependent β -galactosidase activity occurred. CnrX production was checked by Western-blot analysis (WB). Crude extract from 35 μ g dry mass of cells was separated by 15% (w/v) SDS-PAGE, blotted onto a PVDF membrane, and visualized using a polyclonal anti-CnrXs antibody. +, band visible; –, not; ++ strong band (2-fold control). For the MIC determination, the cells were treated as described in the Experimental section. The experiments were reproduced threefold with identical results.

As shown by the Western-blot analysis, strains with *cnrYXH* in the “Yp + Zp” situation produced CnrX independently of the presence of nickel (Fig. 1). This indicates (i) that CnrX production is constitutive due to the action of the *lacZp* promoter upstream of *cnrYp* and (ii) that the CnrX proteins, either wild type or mutants, are stable. In the “Yp – Zp” situation, *cnrYXH* expression and production of the CnrX derivatives depended solely on the ability of the CnrYXH complex to release CnrH for transcription initiation at *cnrYp*. Similar to strain AE126(pMOL28) wild type and DN190 cells carrying wild-type *cnrYXH* on plasmid pBBR1, none of the cells with mutated *cnrX* genes *in trans* produced a CnrX protein in the absence of nickel, except for a faint band visible for the M123C-CnrX mutant. As far as CnrX was concerned, the nickel-dependent regulatory circuits that provided the CnrYXH complex to the cells seemed to be intact in all mutants.

Methionine 123. M123 is essential for CnrX signaling function as previously shown by the phenotype of M123A-CnrX, a mutant protein able to bind nickel similarly to wild type CnrX,

but unable to induce *cnr* expression.²⁶ The M123C-CnrX protein was generated to investigate if the protonated thiol group, a common ligand in metalloproteins, could replace M123 thioether and be able to trigger a nickel-dependent response. Compared to the wild type positive control, the intensity of the M123C-CnrX band was higher than that of the control both in the presence or the absence of Ni(II) in the “Yp + Zp” situation. Otherwise, M123C-CnrX was the only mutant strain producing some CnrX in the absence of nickel in the “Yp – Zp” situation. The basic expression level of β -galactosidase activity was slightly higher than that of the wild type level, *i.e.* sufficient to mediate some nickel resistance and a low level of cobalt resistance. However, no nickel-dependent increase in β -galactosidase activity was observed with M123C-CnrX, in either “Yp + Zp” or “Yp – Zp” situations (Fig. 1). A thiol group provided by a cysteine residue in M123C-CnrX was thus not able to provide the trigger function to CnrX.

Tyrosine 135. Y135 is not in the first coordination sphere of the metal ion in CnrX. It is located in the C-terminal helix of CnrX (helix 4 or h4) and it has been suspected to participate in the interactions with h3 by making a hydrogen bond with Val120.²¹ Moreover, its hydroxyl group points toward the metal-binding site with the hydroxyl oxygen of Y135 just 3.8 Å adjacent to the sulfur atom of the crucial M123. To test whether Y135 is involved in CnrX function, the Y135F mutant was generated, which lacks the hydroxyl group. In the “Yp – Zp” situation, Y135F-CnrXs was associated with a basal nickel-independent reporter activity comparable to that of the negative control. This mutant exhibited a low nickel-dependent increase in reporter activity, along with an approximately two-fold lower metal resistance as compared to WT (Fig. 1). When the mutated *cnrYXH* region was expressed in the “Yp + Zp” situation, the Y135F-CnrX band was twice as strong as that of the control in the presence of Ni(II), similarly to M123C-CnrX. However the nickel-dependent increase in β -galactosidase activity was poor and the resistance to metal ions, especially Co, was severely affected.

Phenylalanine 66. F66 has a high degree of conservation in the CnrX family of proteins.²¹ It belongs to h2 and contributes to interaction with h3 as F66 chain interacts with that of H119 by π – π stacking. Possibly a result of this interaction, H119 is the only metal ligand to display no rearrangement upon metal binding: it has been proposed that F66:H119 stacking maintains the latter in a metal-binding conformation, even in the *apo*-form of the protein.²¹ The F66A mutation was conceived to cancel the π – π interaction with H119. The basal level of β -galactosidase activity was similar to the negative control, and a three-fold decrease was observed in nickel-dependent activity of the reporter compared to WT in either promoter situation. A slight decrease in both nickel and cobalt resistance was observed, indicating that F66 was involved in optimal CnrX function, though inessential.

Nickel and cobalt affinity for CnrXs *in vitro*

The metal binding affinities were determined by chelator competition assays, using the H32A-CnrXs mutant, as previously reported. This mutant form contains only the physiologic metal-binding site and is considered as a wild-type like model.^{21,26} In all cases, data were fit to a single binding-site model. Results are displayed in Table 2 where the previously published dissociation

Table 2 Dissociation constants for Co and Ni determined by competition with the chromogenic chelators fura-2 (H32A- and H32A-Y135F-CnrXs) and mag-fura-2 (H32A-M123A- and H32A-M123C-CnrXs). The statistic value represents the standard deviation to the best fit. The asterisk indicates already published values²⁶

| CnrXs | Co (M) | Ni (M) |
|------------|-----------------------------------|---------------------------------|
| H32A | $6.54 \pm 0.74 \times 10^{-11}$ * | $1.67 \pm 0.15 \times 10^{-12}$ |
| H32A-M123A | $1.11 \pm 0.08 \times 10^{-7}$ * | $8.00 \pm 0.68 \times 10^{-8}$ |
| H32A-M123C | $1.60 \pm 0.19 \times 10^{-7}$ * | $1.33 \pm 0.10 \times 10^{-8}$ |
| H32A-Y135F | $1.10 \pm 0.13 \times 10^{-10}$ | $2.60 \pm 0.32 \times 10^{-12}$ |

constants of Co for H32A-, H32A-M123A-, and H32A-M123C-CnrXs are included for comparison.²⁶ Nickel affinity for H32A-CnrXs, was slightly better than that of cobalt, and the K_d was four orders of magnitude higher for either metal ion when M123 was changed for Ala or Cys. Nickel and cobalt affinity for the WT protein and for H32A-Y135F-CnrXs were in the same range, strongly suggesting that the Y135F mutation preserved the metal-binding site. Consistent with the *in vivo* data reported here and previously,²⁶ nickel affinity measured *in vitro* was constantly higher than Co affinity.

Structural consequences of the mutations

For unknown reasons the crystals of the metal-bound forms of Y135F- and M123C-CnrXs diffracted to a much better resolution

Table 3 Bond distances (Å) to Ni and Co^a

| Refined structure | WT | Y135F | M123C | WT | Y135F |
|--|-------|-------|-------|-------|-------|
| X-ray data resolution (Å) | 1.41 | 1.11 | 1.10 | 1.55 | 1.30 |
| Mean coordinate error ^b (Å) | 0.063 | 0.025 | 0.030 | 0.080 | 0.050 |
| Bound metal | Ni | Ni | Ni | Co | Co |
| His42Nε2 | 2.10 | 2.03 | 2.04 | 2.11 | 2.08 |
| His46Nε2 | 2.12 | 2.08 | 2.07 | 2.11 | 2.13 |
| Glu63Oε1 | 2.20 | 2.14 | 2.19 | 2.13 | 2.16 |
| Glu63Oε2 | 2.23 | 2.13 | 2.13 | 2.16 | 2.16 |
| His119Nε2 | 2.16 | 2.10 | 2.10 | 2.12 | 2.14 |
| M123Sε | 2.45 | 2.47 | | 2.54 | 2.55 |
| Water O | | | 2.10 | | |

^a Using the most ordered molecule 1 for the M123C mutant. ^b Based on resolution and R_{free} .

than all previously obtained crystals (Table 3).^{21,26,44} Because of this, the atomic positions could be determined with unprecedented precision. The omit map electron densities obtained for the Ni-sites show clearly separated peaks for individual ordered atoms. Higher densities for heavier, more electron-rich atoms allow to distinguish N from C and O atoms. In addition to a strong anomalous signal for the Ni, there is a weak one for the most ordered S atoms. Of the two crystallographically independent CnrXs molecules observed in the M123C mutant crystal (Table 1), the second one shows significant disorder. Here the Ni-binding site was tentatively modeled as a 1 : 1 mixture reflecting two Ni positions, as suggested by an elongated peak in the anomalous difference map (Fig. 2C). Because the electron density of the carboxylate group of E63 is rather weak, a second conformation of the protein may exist with a four-coordinate Ni-binding site: H42 (modeled with a flipped imidazole ring), H46, H119 and a water molecule, as shown by the $F_{obs} - F_{calc}$ omit map contour. This might be an artifact resulting from X-ray induced Ni reduction and/or glutamate decarboxylation. Therefore, only one of these conformations was considered relevant *i.e.* the six-coordinate site shown in Fig. 2C.

The Ni-ligand distances are almost the same in the Y135F and M123C mutants except for the replacement of M123Sδ by a water molecule and a 0.05 Å increase of the distance to the opposite apical E63Oε1 ligand (Table 3). For the Co-complex of the Y135F mutant, the average metal-ligand distance is ≈ 0.05 Å higher. This correlates with the observed stronger binding for Ni (Table 2). Except for the M123Sδ-metal distance, a significant difference was not observed for the two metal-bound forms of the WT protein,²¹ but the latter structures were refined at a lower resolution and their mean coordinate error is significantly higher (Table 3).

Remarkably, the Ni-containing forms of WT-CnrXs and its Y135F derivative are almost identical (Table 4). Apparently the mutation did not lead to important structural differences. We therefore decided to analyze and compare also the atomic temperature factors (*B*-factors). Fig. 3 shows that these are lower in the mutant, which suggests that the change of tyrosine by the more hydrophobic phenylalanine has made the structure

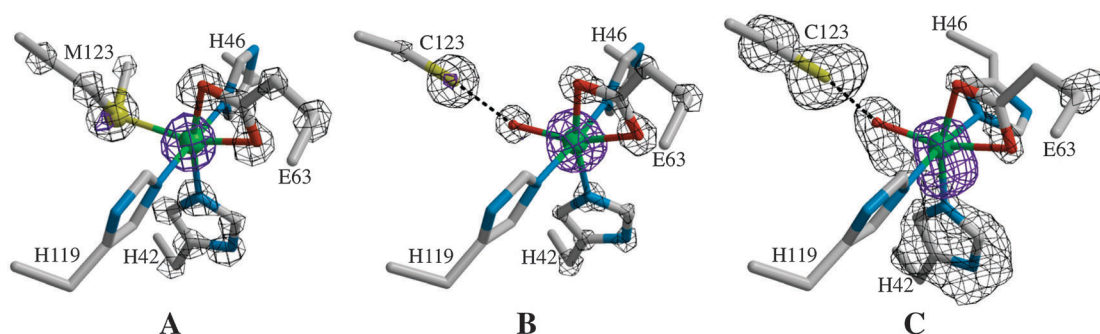


Fig. 2 CnrXs Ni-sites characterized at 1.1 Å resolution in: (A) the Y135F mutant, (B) molecule 1 of the M123C mutant and (C) molecule 2 of the M123C mutant (same crystal). Purple and grey meshes indicate anomalous difference (Δ_{anom}) maps and $F_{obs} - F_{calc}$ omit maps, respectively (the latter show strong peaks only for atoms not included in the model used for refinement). The omit maps are contoured at 10.0, 14.0 and 4.5 σ in (A), (B) and (C), respectively (1 σ corresponds to the root mean square value of the map). All Δ_{anom} maps are contoured at 4.5 σ . Only one conformation is displayed for the disordered Ni-binding site in (C) but the electron density map clearly shows the presence of at least one additional conformation.

Table 4 CnrXs superposition statistics^a for dimers (top-right) and monomers (bottom-left)

| Structure | WT_Ni | Y135F_Ni | M123C_mol1 | M123C_mol2 | WT_Zn |
|------------|-------|----------|------------|------------|-------|
| WT_Ni | — | 0.20 | 1.01 | 1.71 | 2.55 |
| Y135F_Ni | 0.18 | — | 0.96 | 1.79 | 2.57 |
| M123C_mol1 | 0.95 | 0.88 | — | 2.26 | 2.64 |
| M123C_mol2 | 1.41 | 1.51 | 1.96 | — | 2.93 |
| WT_Zn_mol2 | 1.76 | 1.80 | 1.91 | 2.10 | — |
| WT_Zn_mol1 | 2.84 | 2.85 | 2.94 | 2.68 | 2.78 |

^a Arms values using all N, C α , C, O and C β atoms for residues 40–145.

more rigid. Much larger differences are observed with respect to the Zn-bound form of the WT structure, which has much higher *B*-factors and shows a more than ten times higher Δ arms deviation (Table 4).

For the M123C mutant different results are obtained depending on which crystallographically independent molecule is used for the comparison: molecule 1 behaving most like Ni-bound Y135F-CnrXs, but with a five times higher Δ arms deviation with respect to Ni-bound WT. As already discussed, molecule 2 contains a disordered Ni site. This can be recognized also in the relatively high *B*-factors obtained for its N-terminal α -helix (Fig. 3D).

Fig. 4 extends the structural comparisons to the hydrophobic contact interface between the CnrXs monomers in the presumably functional dimeric form. This interface is virtually the same in the Ni-bound forms of WT and Y135F (Fig. 4A). Significant differences are introduced by the mutation of M123 to cysteine. This is shown, for example, by a reorientation of W94 in dimer 1 (Fig. 4B) and by a significant sliding movement of the two subunits in dimer 2 (Fig. 4C). These differences might be correlated by an increase in the separation of the M123-carrying h3 to the Ni site: the distance of the C α atom of residue 123 to Ni is 5.8 Å in WT and Y135F, 6.9 Å in dimer 1 and the main conformation of dimer 2 of M123C, and 7.5 Å in the alternative conformation of the Ni site in dimer 2 of M123C.

Discussion

CnrX, the metal sensor protein of the CnrYXH complex that regulates cobalt and nickel resistance in *C. metallidurans* CH34, responds to metal binding by subtle allosteric modifications depending on the nature of the metal ion.^{21,26} The goal of the present study was to describe the remodeling of the protein at work with respect to its physiological output when it binds Ni(II). This integrated approach combined close-up description of the metal-binding site with description of nickel-dependent secondary or quaternary structural changes, and eventually, the physiological response as a function of selected mutations. High-resolution structures along with the assessment of the nickel affinity for CnrXs, the soluble periplasmic sensor module of CnrX, provided insight of unprecedented clarity on the structural basis of nickel sensing and the first steps of signal propagation.

CnrX is a dimeric protein binding one nickel or cobalt ion per monomer in an octahedral coordination composed of 3 nitrogens from 3 histidines, 2 oxygens from the carboxylate group of a glutamate and the thioether sulfur of the only methionine of the sensor domain of the protein.^{21,26,45} This original coordination sphere requires five different ligands distributed over three of the four helices of this small protein. H42 and H46 are located on the N-terminal h1, E63 is close to the N-terminal end of h2 while H119 and M123 are found in the C-terminal half of h3. This places the metal-binding sites in the midst of a hydrophobic core buried within the four-helix bundle of each protomer. This core region coalesces with the hydrophobic tip of the h2–h3 hairpin of the opposite protomer. The double hydrophobic core hence formed in the CnrX dimer is instrumental in transducing local changes at the metal binding site into metal-dependent conformational changes. Moreover, recent work on the CnrX-homologue NccX has shown that these coalesced hydrophobic cores determine the dimerization of the full length, membrane-embedded protein as well.⁴⁶

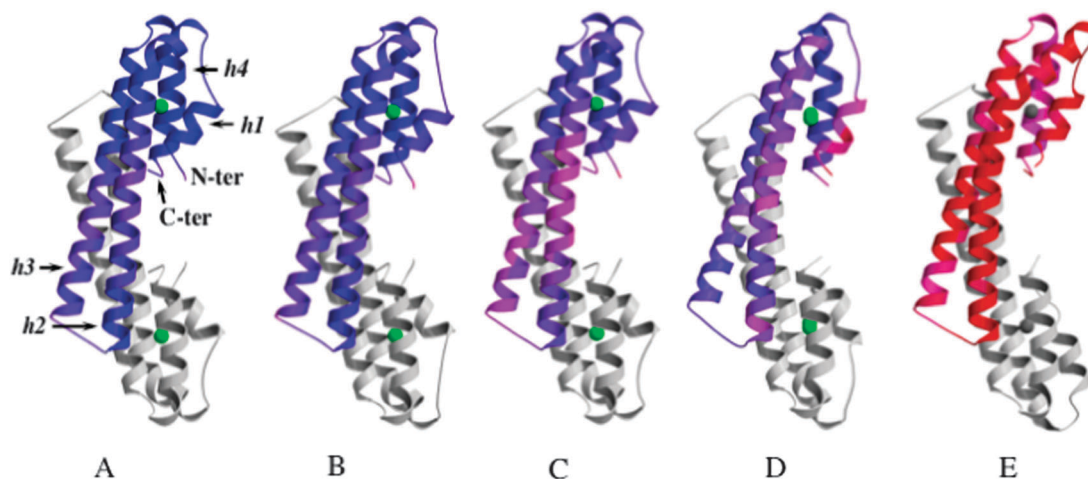


Fig. 3 CnrXs dimers with temperature factors emphasized. (A) Y135F mutant with Ni(II) [9.9 Å² average B factor]. (B) M123C mutant dimer 1 with ordered Ni(II) site [13.1 Å²]. (C) WT with Ni(II) [13.9 Å²]. (D) M123C mutant dimer 2 with disordered Ni(II) site [16.2 Å²]. (E) WT with Zn(II) [46.2 Å²]. Higher B values indicate increased thermal motion. *B*-factors are colored from blue (*B* = 2 Å²) to red (*B* = 40 Å²) in one subunit, α -helices are labeled h1, h2, h3 and h4, metal sites are shown as spheres colored green for Ni and black for Zn.

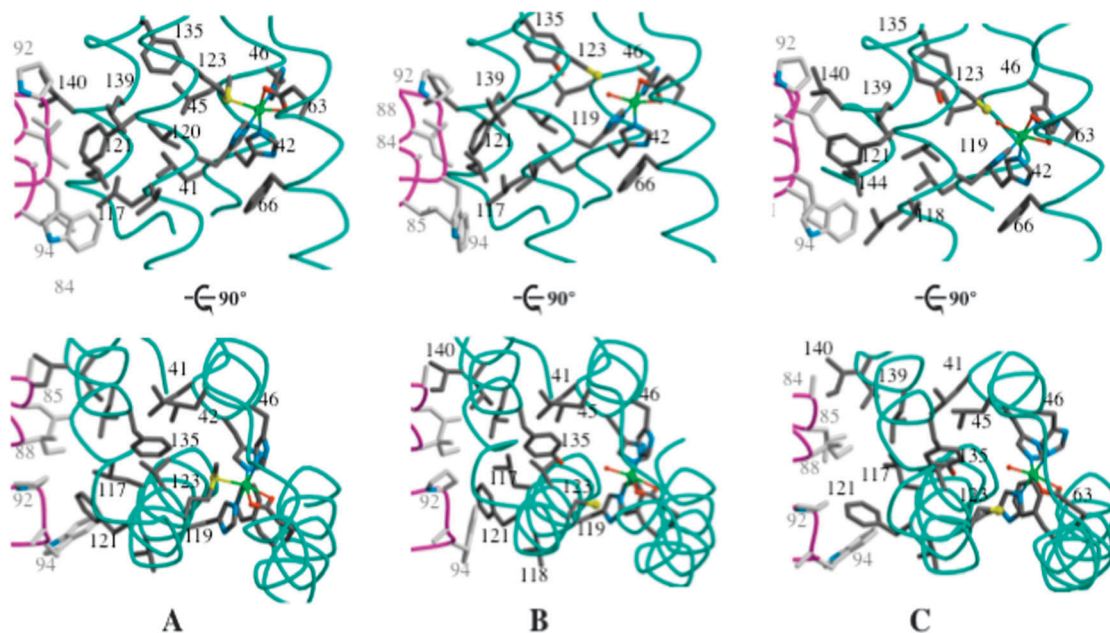


Fig. 4 Hydrophobic contact interface and Ni-site in CnrXs dimers. (A) Y135F mutant. (B) M123C mutant dimer 1. (C) M123C mutant dimer 2. Subunit 1 is colored in cyan (main chain) and gray (C atoms), subunit 2 in pink (main chain) and white (C atoms). Other color codes are green for Ni, yellow for S, red for O and blue for N. Residue numbers are highlighted.

Central in the CnrX protomer architecture is M123 that lies at the bottom of the cavity that harbors the metal ion. This residue is also crucial for the signaling mechanism as its recruitment in the coordination sphere of Ni(II) or Co(II) is the key event that initiates the biological response.²¹ Dissociation constant measurements pointed out the pivotal role of M123 for Co(II) selectivity over Zn(II) that does not use the methionine as a ligand and produces an inactive form of the protein.²⁶ The affinity for Ni(II) was now determined for the wild-type surrogate of CnrXs (H32A) and its M123A, M123C and Y135F derivatives. The affinities for Ni(II) were 10- to 100-fold higher than the affinities for Co(II). Changing M123 for an alanine or a cysteine caused the decrease of the affinity for Ni(II) by four orders of magnitude consistently with the difference already observed for Co(II). This is in agreement with transcriptomic, proteomic and *in vivo* data indicating that nickel is a better inducer of *cnr* than cobalt. The weaker binding of Co(II) is probably related to the larger metal–ligand distances compared to Ni(II) as could be measured with confidence in the atomic-resolution structures of Y135F-CnrXs in which the metal-binding site was preserved. Stronger interaction and tighter ligand binding are easily observed with Ni(II) vs. Co(II). For instance, distances found for six-coordinate Co(II) complexes (3N₃O or 4N₂O) from the Cambridge Structural Database (<http://www.ccdc.cam.ac.uk/products/csd/>) are generally longer compared to their Ni(II) counterpart (data not shown). These data also fit with a larger ionic radius for Co(II): the ionic radii of six-coordinate high-spin Co(II) and Ni(II) are 0.885 Å and 0.83 Å, respectively.⁴⁷ As far as nickel and cobalt are concerned, higher affinities for Ni(II) than Co(II) are also consistent with the trend in the Irving Williams series, for which the relative stability of a complex formed by a metal ion follows the order Co(II) < Ni(II).⁴⁸

Accordingly, a microbial biosensor based on the transcriptional fusion of the regulatory genes *cnrYXH* upstream of the *lux* operon was applicable to the detection of Ni(II) in the range 0.1–60 µM and of Co(II) between 9 and 400 µM, making the sensitivity of this biosensor 100-fold greater for nickel compared to cobalt.⁴⁹ It is noteworthy that all the mutants characterized in this study were more significantly altered with respect to cobalt-induced resistance than to nickel-induced resistance (MIC, Fig. 1), showing that the functionality of CnrX is more robust as far as Ni(II) is concerned. Accordingly, Cnr plays a minor role in *C. metallidurans* resistance to Co(II), which relies on *Czc* instead.²² This suggests that CnrX sensitivity may have been tuned for Ni(II) sensing, maybe because Co(II) did not exert a selective pressure on *cnrX*.

The physiological data pinpointed differentiated phenotypes of the mutants regarding Ni(II)- and Co(II)-dependent *cnrCBA* induction. In contrast, the crystal structures of Y135F-CnrXs metallated with Ni(II) or Co(II) were perfectly superimposable to each other and were superimposable to Ni(II)-bound wild-type CnrXs with the best fit ever calculated for any other form crystallized so far ($\Delta r_{\text{rms}} = 0.20$ Å, Table 4). This is consistent with Y135F-CnrXs being somewhat functional *in vivo*, although the mutant was less active than the wild type. The basis of this limited effect was thus sought in the agitation parameters rather than in the molecular models themselves. With the average *B*-factors as indicators of the flexibility of the molecules and Ni-bound WT-CnrXs as a reference for an active sensor, partially active Ni-bound Y135F CnrXs was found more rigid, and the very flexible Zn-bound WT-CnrXs is inactive (Fig. 3). According to the same parameters, inactive Ni-bound M123C-CnrXs dimers were either more rigid (dimer 1) or less rigid (dimer 2) than WT-CnrXs, suggesting that flexibility should be

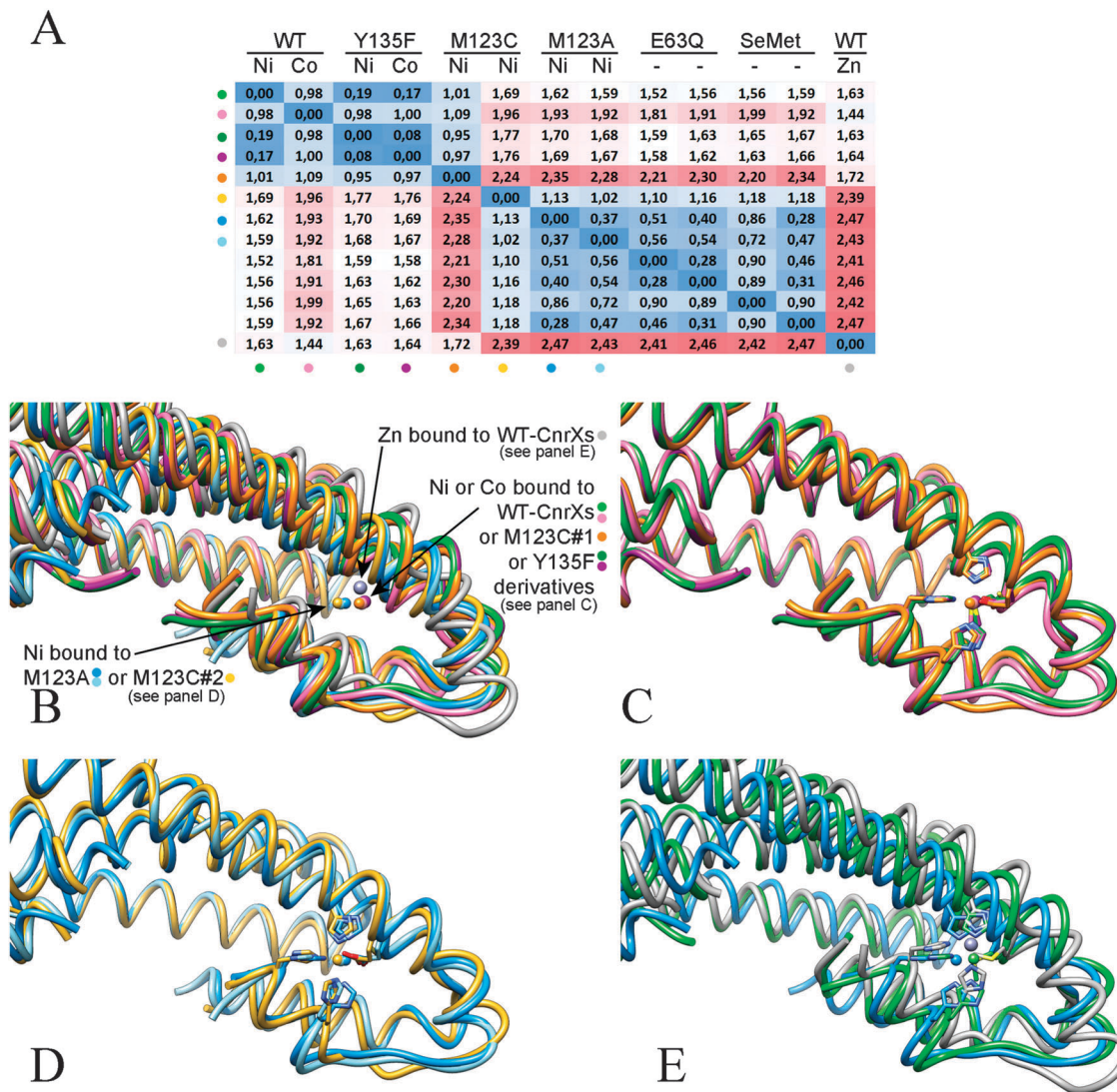


Fig. 5 Structural superimposition of CnrXs various conformations. Panel A: CnrXs dimeric structures determined here and previously published have been superimposed.^{21,26} A structural alignment was produced for chains aligned with Ni-bound CnrXs chain B and the calculated rmsd's have been reported as a matrix. Blue-to-white-to-red shading was applied automatically with Excel over the complete table. Three ranges were identified. One gathered Ni-bound CnrXs, Co-bound CnrXs, Ni-bound Y135F-CnrXs, Co-bound Y135F-CnrXs and Ni-bound M123C-CnrXs-D (dimer 1 = AD). The second gathered the Ni-bound forms of M123C-C, M123A-A, M123A-C, and apo-forms of CnrXs as present in either E63Q-CnrXs or SeMet-CnrXs dimers.²¹ Finally, WT-Zn aligned poorly with all other structures. As a result, three conformational states are observed. Panel B: close-up view at the metal ions bound to superimposed CnrXs dimers. Each ion was colored as the protein chain. The color code is displayed in both entries of the table in panel A. Metal ions clustered the same way as the protein chains. Panel C: an "active" conformational state with Co or Ni in CnrXs WT, Y135F, and M123C dimer 1. Panel D: an "artificial" conformational state observed in M123A and M123C mutants. Panel E: a Zn-bound conformational state (grey) displayed together with superimposed Ni-bound CnrXs and (green) and Ni-bound M123A-CnrXs (blue) for comparison. Structures were generated with UCSF Chimera.⁵⁴

neither too low nor too high for optimal functionality. The phenotype of the Y135F mutant might be explained by the increased hydrophobicity of the phenylalanine side-chain making the structure too rigid. This interpretation echoes previous work on M123A-CnrXs, suggested to be defective in metal-dependent allosteric switching.²⁶ With the high-resolution structure of Ni-bound M123C-CnrXs now also determined, the roles of M123 in both conformational flexibility and CnrX function was confirmed. Because of the loss of this crucial sixth ligand, M123C- and M123A-CnrXs were unable to propagate any signal despite metallation.

Signal-silent forms seemed either too rigid or too relaxed, thus confirming the suggestion that CnrX couples metal binding to signal propagation *via* the packing of its hydrophobic core and that a hinge in the hairpin contributes to regulate the compactness of the dimer.²¹ Regarding F66, of the two roles previously assigned to this residue,²¹ one was to help maintaining the side-chain of H119 in a metal-binding conformation by π - π stacking, and the other was to serve as a hinge permitting the lateral movement of the N-terminal part of h2 during the switch between the unproductive Zn-bound form and the active Ni- or Co-bound form. In the absence of an X-ray

structure, we speculate that the alanine residue in the F66A mutation cannot correctly fulfill either of these roles, thus explaining the diminished nickel-sensitivity of this mutant.

A remarkable effect of the M123 substitutions was the unusually blue-shifted visible spectrum, either in the Co- or the Ni-bound forms. The comparison of these spectra suggested that a cysteine in position 123 was not a ligand of the metal ion.²⁶ This prediction is now confirmed by the crystallographic data. As already observed for the M123A mutation, the Ni ion remains six-coordinate in Ni-bound M123C-CnrXs, the thioether sulfur being replaced by a water molecule as the sixth ligand. Using the structure of the most ordered molecule 1, the thiolate sulfur of C123 is placed at 3.3 Å from the water molecule with which it forms a hydrogen bond.

Two different copies of the molecule were found in the asymmetric unit, so that the crystals of Ni-bound M123C-CnrXs appeared to be built from two types of dimers. Both types displayed different conformations and thermal agitation parameters, dimer 1 being better defined than dimer 2. The low omit map density for the side chain of E63 in dimer 2 suggests that either this residue is partially decarboxylated, due to X-ray damage, or that putative alternative conformations not bound to the metal are disordered and therefore not resolved in the electron density map. Ni(II) might also be reduced to Ni(I) by X-ray photo-electrons. At a resolution of 1.1 Å, the confidence in the conformations determined is high. Interestingly they differ significantly from each other. This is unlike what had been observed with crystallized *apo*-forms of CnrXs (e.g. E63Q-CnrXs or the selenomethionyl derivative of wild-type CnrXs) whose crystals contained four marginally different chains (two dimers) per asymmetric unit.²¹ Mutual structural superimpositions were performed within a comprehensive collection of CnrXs dimers (Fig. 5). Rmsd's were computed for single chains, which allowed defining three conformational groups (Fig. 5, panel A). While one M123C chain clustered with Ni(II)- and Co(II)-bound forms of wild type and Y135F-CnrXs, *i.e.* active forms, the second M123C chain clustered with *apo*-forms of CnrXs and M123A-CnrXs. Wild type Zn(II)-bound CnrXs did not cluster with any other chain and made a third group on its own. When the various dimers of metallated CnrXs were superimposed, the same pattern was obtained based on the relative positions of the bound metal ions (Fig. 5, panel B). This indicated that the conformations crystallized for CnrXs belong to discrete states: the active state (Fig. 5, panel C), an artifactual state induced by the mutation of M123 to Ala or Cys (Fig. 5, panel D) and the resting state (Fig. 5, panel E). Most significant is the fact that Ni(II)-bound M123C-CnrXs crystallized as two dimers with conformations similar to those already characterized in different crystallographic systems, because this ascertained the relevance of the conformations crystallized. Furthermore, this substantiates the hypothesis that significantly different conformations of CnrXs may coexist in solution and that Ni(II) may bind several of them. This suggests that nickel sensing would proceed *via* conformational selection,⁵⁰ possibly driven by the recruitment of M123.

Events downstream metal sensing by CnrX remains to be investigated. Recent *in vivo* and *in silico* data have shown that

the transmembrane segments of isolated NccX, a close CnrX homologue, engage in highly dynamic self-interactions,⁴⁶ which indicates that they might not support signaling on their own. The characterization of the interaction between CnrH and CnrY cytosolic domain also suggested that CnrY would probably not propagate a conformational change.²⁵ By analogy with known activation modes of ECF sigma factors in response to envelope stress, CnrH release might proceed from the post-translational modification or proteolytic processing of CnrY.^{51–53} Understanding how metal-induced conformational selection at the CnrX periplasmic domain prompts CnrH release in the cytoplasm therefore requires further work to characterize the CnrX:CnrY interaction.

Abbreviations

| | |
|--------------|---|
| Δanom | Anomalous difference |
| ECF | Extracytoplasmic function |
| MIC | Minimum inhibitory concentration |
| RMSD or Δrms | Root-mean-square deviation |
| RND | Resistance nodulation and cell division |
| TMM | Tris-buffered mineral salts medium |
| WT | Wild type |

Acknowledgements

We thank Eric Girard and Juan Fontecilla-Camps for their contribution to the first steps of X-ray data collection and structure determination. Géraldine Sarret is thanked for providing us with interatomic distances for Co(II)- and Ni(II)-complexes extracted from the Cambridge structural database.

References

- 1 R. P. Hausinger and D. B. Zamble, in *Molecular Microbiology of heavy metals*, ed. D. H. Nies and S. Silver, Springer-Verlag, Berlin, 2007, pp. 287–320.
- 2 J. L. Boer, S. B. Mulroone and R. P. Hausinger, *Arch. Biochem. Biophys.*, 2014, **544**, 142–152.
- 3 L. Macomber and R. P. Hausinger, *Metallomics*, 2011, **3**, 1153–1162.
- 4 L. Macomber, S. P. Elsey and R. P. Hausinger, *Mol. Microbiol.*, 2011, **82**, 1291–1300.
- 5 M. Kobayashi and S. Shimizu, *Eur. J. Biochem.*, 1999, **261**, 1–9.
- 6 T. Majtan, F. E. Frerman and J. P. Kraus, *BioMetals*, 2011, **24**, 335–347.
- 7 J. R. Fantino, B. Py, M. Fontecave and F. Barras, *Environ. Microbiol.*, 2010, **12**, 2846–2857.
- 8 M. P. Thorgersen and D. M. Downs, *J. Bacteriol.*, 2007, **189**, 7774–7781.
- 9 C. Ranquet, S. Ollagnier-de-Choudens, L. Loiseau, F. Barras and M. Fontecave, *J. Biol. Chem.*, 2007, **282**, 30442–30451.
- 10 J. S. Iwig, J. L. Rowe and P. T. Chivers, *Mol. Microbiol.*, 2006, **62**, 252–262.

- 11 D. Koch, D. H. Nies and G. Grass, *BioMetals*, 2007, **20**, 759–771.
- 12 P. T. Chivers and R. T. Sauer, *Protein Sci.*, 1999, **8**, 2494–2500.
- 13 K. De Pina, V. Desjardin, M.-A. Mandrand-Berthelot, G. Giordano and L. F. Wu, *J. Bacteriol.*, 1999, **181**, 670–674.
- 14 S. Leitch, M. J. Bradley, J. L. Rowe, P. T. Chivers and M. J. Maroney, *J. Am. Chem. Soc.*, 2007, **129**, 5085–5095.
- 15 A. Rodrigue, G. Effantin and M.-A. Mandrand-Berthelot, *J. Bacteriol.*, 2005, **187**, 2912–2916.
- 16 A. Kirsten, M. Herzberg, A. Voigt, J. Seravalli, G. Grass, J. Scherer and D. H. Nies, *J. Bacteriol.*, 2011, **193**, 4652–4663.
- 17 D. Munkelt, G. Grass and D. H. Nies, *J. Bacteriol.*, 2004, **186**, 8036–8043.
- 18 H. Liesegang, K. Lemke, R. A. Siddiqui and H.-G. Schlegel, *J. Bacteriol.*, 1993, **175**, 767–778.
- 19 S. Monchy, M. A. Benotmane, P. Janssen, T. Vallaey, S. Taghavi, D. van der Lelie and M. Mergeay, *J. Bacteriol.*, 2007, **189**, 7417–7425.
- 20 G. Grass, C. Grosse and D. H. Nies, *J. Bacteriol.*, 2000, **182**, 1390–1398.
- 21 J. Trepreau, E. Girard, A. P. Maillard, E. de Rosny, I. Petit-Haertlein, R. Kahn and J. Covès, *J. Mol. Biol.*, 2011, **408**, 408–766.
- 22 D. H. Nies, G. Rehbein, T. Hoffmann, C. Baumann and C. Grosse, *J. Mol. Microbiol. Biotechnol.*, 2006, **11**, 82–93.
- 23 C. Tibazarwa, S. Wuertz, M. Mergeay, L. Wyns and D. van der Lelie, *J. Bacteriol.*, 2000, **182**, 1399–1409.
- 24 G. Grass, B. Fricke and D. H. Nies, *BioMetals*, 2005, **18**, 437–448.
- 25 A. P. Maillard, E. Girard, W. Ziani, I. Petit-Härtlein, R. Kahn and J. Covès, *J. Mol. Biol.*, 2014, **426**, 2313–2327.
- 26 J. Trepreau, C. Grosse, J.-M. Mouesca, G. Sarret, E. Girard, I. Petit-Härtlein, S. Künnemann, C. Desbourdes, E. de Rosny, A. P. Maillard, D. H. Nies and J. Covès, *Metallomics*, 2014, **6**, 263–273.
- 27 K. J. Waldron, J. C. Rutherford, D. Ford and N. J. Robinson, *Nature*, 2009, **460**, 823–830.
- 28 H. Reyes-Caballero, G. C. Campanello and D. P. Robinson, *Biophys. Chem.*, 2011, **156**, 103–114.
- 29 N. E. Grosseohme and D. P. Giedroc, *Methods Mol. Biol.*, 2012, **796**, 31–51.
- 30 M. Mergeay, D. H. Nies, H. G. Schlegel, J. Gerits, P. Charles and F. van Gijsegem, *J. Bacteriol.*, 1985, **162**, 328–334.
- 31 D. H. Nies, M. Mergeay, B. Friedrich and H. G. Schlegel, *J. Bacteriol.*, 1987, **169**, 4865–4868.
- 32 J. Sambrook, E. F. Fritsch and T. Maniatis, *Molecular cloning, a laboratory manual*, Cold Spring Harbor Laboratory, Cold Spring Harbor, NY, 1989.
- 33 R. Simon, U. B. Priefer and A. Pühler, *Nat. Biotechnol.*, 1983, **1**, 784–791.
- 34 D. H. Nies, *J. Bacteriol.*, 1992, **174**, 8102–8110.
- 35 M. M. Bradford, *Anal. Biochem.*, 1976, **72**, 248–254.
- 36 P. Kuzmic, *Methods Enzymol.*, 2009, **467**, 247–280.
- 37 M. V. Golynskiy, W. A. Gunderson, M. P. Hendrich and S. M. Cohen, *Biochemistry*, 2006, **45**, 15359–15372.
- 38 W. Kabsch, *Acta Crystallogr., Sect. D: Biol. Crystallogr.*, 2010, **66**, 125–132.
- 39 M. D. Winn, C. C. Ballard, K. D. Cowtan, E. J. Dodson, P. Emsley, P. R. Evans, R. M. Keegan, E. B. Krissinel, A. G. W. Leslie, A. McCoy, S. J. McNicholas, G. N. Murshudov, N. S. Pannu, E. A. Potterton, H. R. Powell, R. J. Read, A. Vagin and K. S. Wilson, *Acta Crystallogr., Sect. D: Biol. Crystallogr.*, 2011, **67**, 235–242.
- 40 A. J. McCoy, R. W. Grosse-Kunstleve, P. D. Adams, M. D. Winn, L. C. Storoni and R. J. Read, *J. Appl. Crystallogr.*, 2007, **40**, 658–674.
- 41 T. C. Terwilliger, R. W. Grosse-Kunstleve, P. V. Afonine, N. W. Moriarty, P. H. Zwart, L.-W. Hung, R. J. Read and P. D. Adams, *Acta Crystallogr., Sect. D: Biol. Crystallogr.*, 2008, **64**, 61–69.
- 42 G. N. Murshudov, P. Skubak, A. A. Lebedev, N. S. Pannu, R. A. Steiner, R. A. Nicholls, M. D. Winn, F. Long and A. A. Vagin, *Acta Crystallogr., Sect. D: Biol. Crystallogr.*, 2011, **67**, 355–367.
- 43 P. Emsley, B. Lohkamp, W. G. Scott and K. Cowtan, *Acta Crystallogr., Sect. D: Biol. Crystallogr.*, 2010, **66**, 486–501.
- 44 G. Pompidor, A. P. Maillard, E. Girard, S. Gambarelli, R. Kahn and J. Covès, *FEBS Lett.*, 2008, **582**, 3954–3958.
- 45 J. Trepreau, E. de Rosny, C. Duboc, G. Sarret, I. Petit-Härtlein, A. P. Maillard, A. Imberty, O. Proux and J. Covès, *Biochemistry*, 2011, **50**, 9036–9045.
- 46 W. Ziani, A. P. Maillard, I. Petit-Härtlein, N. Garnier, S. Crouzy, E. Girard and J. Covès, *J. Biol. Chem.*, 2014, **289**, 31160–31172.
- 47 R. D. Shannon, *Acta Crystallogr., Sect. A: Cryst. Phys., Diffraction, Theor. Gen. Crystallogr.*, 1976, **32**, 751–767.
- 48 H. Irving and R. J. P. Williams, *J. Chem. Soc.*, 1953, 3192–3210.
- 49 C. Tibazarwa, P. Corbisier, M. Mench, A. Bossus, M. Mergeay, L. Wyns and D. van der Lelie, *Environ. Pollut.*, 2001, **113**, 19–26.
- 50 D. D. Boehr, R. Nussinov and P. E. Wright, *Nat. Chem. Biol.*, 2009, **5**, 789–796.
- 51 B. G. Butcher, T. Masher and J. D. Helmann, in *Bacterial physiology, a molecular approach*, ed. W. El-Sharoud, Springer-Verlag GmbH, Berlin, Heidelberg, 2008.
- 52 J. Heinrich and T. Wiegert, *Res. Microbiol.*, 2009, **160**, 696–703.
- 53 A. Staroń and T. Mascher, *Microbe*, 2010, **5**, 164–170.
- 54 E. F. Pettersen, T. D. Goddard, C. C. Huang, G. S. Couch, D. M. Greenblatt, E. C. Meng and T. E. Ferrin, *J. Comput. Chem.*, 2004, **25**, 1605–1612.